VIROLOGY

Human SAMD9 is a poxvirus-activatable anticodon nuclease inhibiting codon-specific protein synthesis

Fushun Zhang[1], Quanquan Ji[2], Juhi Chaturvedi[3], Marisol Morales[1], Yuanhui Mao[2], Xiangzhi Meng[1], Leiming Dong[2], Junpeng Deng[3], Shu-Bing Qian[2]*, Yan Xiang[1]*

As a defense strategy against viruses or competitors, some microbes use anticodon nucleases (ACNases) to deplete essential tRNAs, effectively halting global protein synthesis. However, this mechanism has not been observed in multicellular eukaryotes. Here, we report that human SAMD9 is an ACNase that specifically cleaves phenylalanine tRNA (tRNA^{Phe}), resulting in codon-specific ribosomal pausing and stress signaling. While SAMD9 ACNase activity is normally latent in cells, it can be activated by poxvirus infection or rendered constitutively active by SAMD9 mutations associated with various human disorders, revealing tRNA^{Phe} depletion as an antiviral mechanism and a pathogenic condition in SAMD9 disorders. We identified the N-terminal effector domain of SAMD9 as the ACNase, with substrate specificity primarily determined by a eukaryotic tRNA^{Phe}–specific 2′-*O*-methylation at the wobble position, making virtually all eukaryotic tRNA^{Phe} susceptible to SAMD9 cleavage. Notably, the structure and substrate specificity of SAMD9 ACNase differ from known microbial ACNases, suggesting convergent evolution of a common immune defense strategy targeting tRNAs.

INTRODUCTION

Transfer RNAs (tRNAs) are one of the most conserved components of protein synthesis machinery. They are also a major target for protein toxins used by microbes to impede virus infection, mitigate cellular stress, or eliminate competing organisms (*1*). Many tRNA-targeting protein toxins are anticodon nucleases (ACNases) that cleave at the anticodon stem loops (ASLs), leading to depletion of specific tRNAs from cellular pools and a block in protein synthesis. Notable examples of ACNases include *Escherichia coli* PrrC, which is activated upon T4 phage infection and serves as an innate defense against phages (*2*), and *E. coli* Colicin E5 (*1*) and *Kluyveromyces lactis* γ-toxin (*3*), which are secreted from producing cells to arrest growth of competing bacterial or yeast cells. tRNA cleavage is also associated with some stress responses in eukaryotic cells (*4*), but the cleavage does not substantially reduce cellular tRNA pools, and no tRNA-depleting ACNases have been reported for multicellular eukaryotes.

In vertebrate animals, interferon-regulated innate immune system serves as the first line of defense against viruses, and innate antiviral factors can pose as host restriction factors that block the replication of certain groups of viruses. A paralogous pair of mammalian interferon-stimulated gene products, sterile alpha motif domain–containing 9 (SAMD9) and SAMD9-like (SAMD9L) (SAMD9/9L), are potent restriction factors for poxviruses (*5*–*7*), a family of DNA viruses that include monkeypox virus and vaccinia virus (VACV). Conversely, mammalian poxviruses have evolved multiple inhibitors of SAMD9/9L (*5*, *6*, *8*, *9*), without which they would fail to replicate in mammalian cells due to a block in protein synthesis (*10*–*12*). In addition to their antiviral activities, SAMD9/9L also have antiproliferative activities. Germline mutations in SAMD9/9L cause a range of human diseases, including around 10% of the inherited bone marrow failure syndromes (*13*, *14*) and several rare multisystem disorders (*15*–*17*). The mutations are mostly missense mutations that result in a gain of function (GoF) in inhibition of cell proliferation (*14*, *15*) and protein synthesis (*18*–*20*).

SAMD9/9L are ubiquitously expressed cytosolic proteins with a predicted domain architecture (*21*) resembling that of the STAND (signal transduction adenosine triphosphatases with numerous associated domains) (*22*) superfamily of immune sensors, which includes the nucleotide-binding oligomerization domain (NOD)–like receptors (*23*). STAND proteins share a conserved tripartite domain architecture, consisting of a C-terminal sensor that recognizes danger- or pathogen-associated molecular patterns (PAMPs), a central NOD that mediates the formation of a supramolecular complex, and an N-terminal effector that is allosterically activated to exert the downstream effect. Consistently, an N-terminal effector domain was recently identified in SAMD9/9L, and its functions were found to be closely linked to its ability to bind double-stranded nucleic acid (dsNA) in vitro (*18*). In this study, we found how SAMD9/9L inhibit viral replication and protein synthesis with the effector domain, which unexpectedly shares a functional connection with microbial ACNases.

RESULTS

FTSJ1-mediated 2′-*O*-methylation of tRNA wobble position is critical for host restriction of VACV

SAMD9, WD repeat domain 6 (WDR6), and FtsJ RNA 2′-*O*-methyltransferase 1 (FTSJ1) were previously identified by a human genome-wide RNA interference screen (*6*) and subsequently confirmed with individual gene knockout in HeLa cells (*11*), as host restriction factors for a VACV mutant that lacks two viral SAMD9/9L inhibitors (*7*) (referred to as vK1^{-}C7^{-}). However, how they are connected in restricting VACV was unknown. FTSJ1 is an RNA

[1]Department of Microbiology, Immunology and Molecular Genetics, University of Texas Health Science Center at San Antonio, 7703 Floyd Curl Drive, San Antonio, TX 78229, USA. [2]Division of Nutritional Sciences, Cornell University, Ithaca, NY 14853, USA. [3]Department of Biochemistry and Molecular Biology, Oklahoma State University, 246 Noble Research Center, Stillwater, OK 74078, USA.
*Corresponding author. Email: xiangy@uthscsa.edu (Y.X.); sq38@cornell.edu (S.-B. Q.)

methyltransferase that interacts separately with thyroid adenoma-associated protein (THADA) and WDR6 to install 2′-*O*-ribose methylation at positions 32 and 34 of certain tRNA species (*24*), respectively. The coidentification of WDR6 but not THADA from the same genome-wide screen suggests that tRNA methylation at position 34 is important for the host restriction. To test this idea, we knocked out *FTSJ1* from HeLa cells and reconstituted the *FTSJ1* KO cells (ΔFTSJ1) with a Dox-inducible *FTSJ1* allele. As expected, FTSJ1-deficient cells failed to restrict vK1$^-$C7$^-$. Induction of *FTSJ1*–wild type (WT) expression to different levels restored the restriction in a dose-dependent manner (Fig. 1A). By contrast, *FTSJ1* with K28A or A26P mutation failed to restore the restriction (Fig. 1B). The K28A mutation of the catalytic site completely inactivates the methyltransferase activity, while the A26P mutation specifically disrupts methylation at position 34 but leaves methylation at position 32 intact (*25*). These results indicate that 2′-*O*-methylation at position 34—the wobble position of the anticodon—is critical for host restriction of vK1$^-$C7$^-$.

SAMD9 is a VACV-activatable endoribonuclease with an exquisite specificity for 2′-*O*-methylated tRNA^{Phe}

In human cells, tRNA^{Phe}, tryptophan tRNA (tRNA^{Trp}), and leucine tRNA with CAA anticodon (tRNA$^{Leu(CAA)}$) are known to be methylated at position 34 by FTSJ1 (*26*, *27*). Among them, tRNA^{Phe} has been identified as the most biologically important substrate for FTSJ1 across eukaryotes (*26*, *28*). We thus focused on tRNA^{Phe} to decipher the functional connection between SAMD9 and FTSJ1/WDR6 in host restriction of vK1$^-$C7$^-$. We infected WT and ΔFTSJ1 HeLa cells with vK1$^-$C7$^-$ and analyzed tRNA^{Phe} by Northern blot (Fig. 1C). In WT HeLa cells, tRNA^{Phe} level decreased continuously during the first few hours of infection, reaching a steady state of ~40 to 50% of the original level by 4 to 6 hours postinfection (hpi). Two tRNA^{Phe} fragments appeared at 2 hpi when full-length (FL) tRNA^{Phe} level was still relatively high, suggesting that tRNA^{Phe} was cleaved into two fragments before being completely degraded. The degradation only requires the early phase of viral replication, as it was not affected when replication was blocked at genome replication by cytosine arabinoside (AraC). In ΔFTSJ1 cells, tRNA^{Phe} level was also reduced after vK1$^-$C7$^-$ infection, but the degree of reduction was relatively small. tRNA^{Phe} was not degraded in HeLa cells after WT VACV infection or in SAMD9 and SAMD9L KO (ΔSAMD9&L) cells after vK1$^-$C7$^-$ infection (shown later), indicating that SAMD9 or SAMD9L is required for the degradation.

We recently identified an effector domain in SAMD9/9L that binds to dsNAs (*18*). Given that tRNA is highly structured and contains many ds regions, we reasoned that this effector domain was responsible for degrading tRNA^{Phe}. The incubation of recombinant SAMD9$^{134–385}$ protein with total RNA from HeLa cells produced two distinct RNA fragments, which were abundant enough to be visualized with only nucleic acid staining (Fig. 1C). Northern blot identified the large [~50 nucleotides (nt)] and the small (~30 nt) fragments to be 3′ and 5′ end of tRNA^{Phe}, respectively. They were identical in size to the two tRNA^{Phe} fragments transiently present in infected cells. With increasing incubation time, an increasing amount of tRNA^{Phe} was cleaved by SAMD9$^{134–385}$, but the cleavage products were not degraded (Fig. 1D), suggesting that further degradation of tRNA fragments in infected cells is likely mediated by a separate exonuclease. Notably, tRNA$^{Leu(CAA)}$ as well as six other tRNAs that we specifically tested for were not cleaved by SAMD9$^{134–385}$ or degraded in cells infected with vK1$^-$C7$^-$ (Fig. 1C and fig. S1). SAMD9$^{134–385}$ did not cleave tRNA^{Phe} from ΔFTSJ1 cells under our in vitro assay condition (Fig. 1E), indicating that tRNA 2′-*O*-methylation is critical for substrate specificity. Because of its unique specificity for 2′-*O*-methylated tRNA^{Phe}, we named the SAMD9 effector domain (SAMD9$^{134–385}$) tRNA ribonuclease (tRNase) SA (for SAMD9/9L).

tRNA binding and active site of tRNase SA

We previously solved the crystal structure of SAMD9$^{156–385}$ in complex with DNA and identified a dsNA binding site that is essential for antiviral and antiproliferative activities of SAMD9 (Fig. 2A) (*18*). With a gel mobility shift assay, we found that tRNase SA formed a stable complex with purified yeast tRNA^{Phe}, and the binding is mediated by the previously identified dsNA binding residues, including K198, K214, and R221. Specifically, K198E, K214E, and R221E mutations abolished, while K350E and K242E mutations reduced the binding (Fig. 2B). Consistently, these mutations affected the cleavage of human tRNA^{Phe} by tRNase SA to different degrees (Fig. 2C).

We found that a divalent cation is required for tRNase SA cleavage of tRNA^{Phe}. While Mn^{2+} is preferred over Mg^{2+}, Ca^{2+} and Zn^{2+} do not support the cleavage of tRNA^{Phe} (Fig. 2D). This rather stringent selection of divalent cation is a characteristic of nucleases that use two metal ions, coordinated by acidic residues, for catalysis (*29*). Upon close examination of the structure of SAMD9$^{156–385}$/dsDNA complex, we identified a cluster of conserved acidic residues on the protein′s surface near the dsNA binding site (Fig. 2A and fig. S2A). To investigate whether this cluster could represent the active site, we performed mutagenesis studies on these residues. In SAMD9, D345A substitution had no significant effect on its antiviral activity against VACV, while D192A partially reduced the antiviral activity (Fig. 2E). Furthermore, E184A, E196A, E218A, and D241A substitutions resulted in complete loss of the antiviral activity (Fig. 2E), indicating that these four acidic residues are essential for SAMD9 function. Recombinant SAMD9$^{156–385}$ proteins with E184A, E196A, E218A, or D241A substitutions could be purified similarly to the WT version and exhibited comparable binding to yeast tRNA^{Phe} (Fig. 2B), suggesting that the mutations do not affect protein folding. However, the mutations abolished the cleavage of human tRNA^{Phe} (Fig. 2C). These data collectively support the idea that E184, E196, E218, and D241 serve as the active site residues for tRNase SA in SAMD9.

tRNase SA targets the ASL with a 2′-*O*-methylguanosine

While tRNase SA forms a stable complex with yeast tRNA^{Phe} at 4°C with no sign of cleavage (Fig. 2B), we found that it cleaves yeast tRNA^{Phe} at 37°C (fig. S3A). To identify the cleavage site, we isolated the cleavage products and determined their molecular weights (MWs) by mass spectrometry (fig. S3A). This analysis revealed that SAMD9$^{134–385}$ cleaves between nucleotides 31 and 32, producing termini with 5′-phosphate and 3′-OH. We next examined the cleavage products using total RNAs from HeLa cells. Only the small cleavage product was purified with sufficient quantity for MW determination, and it belongs to the first 31 nucleotides of human tRNA^{Phe} with a 3′-OH (fig. S3A). Therefore, tRNase SA specifically cleaves tRNA^{Phe} among the numerous RNA species in human cells by targeting the same cleavage site as that of yeast

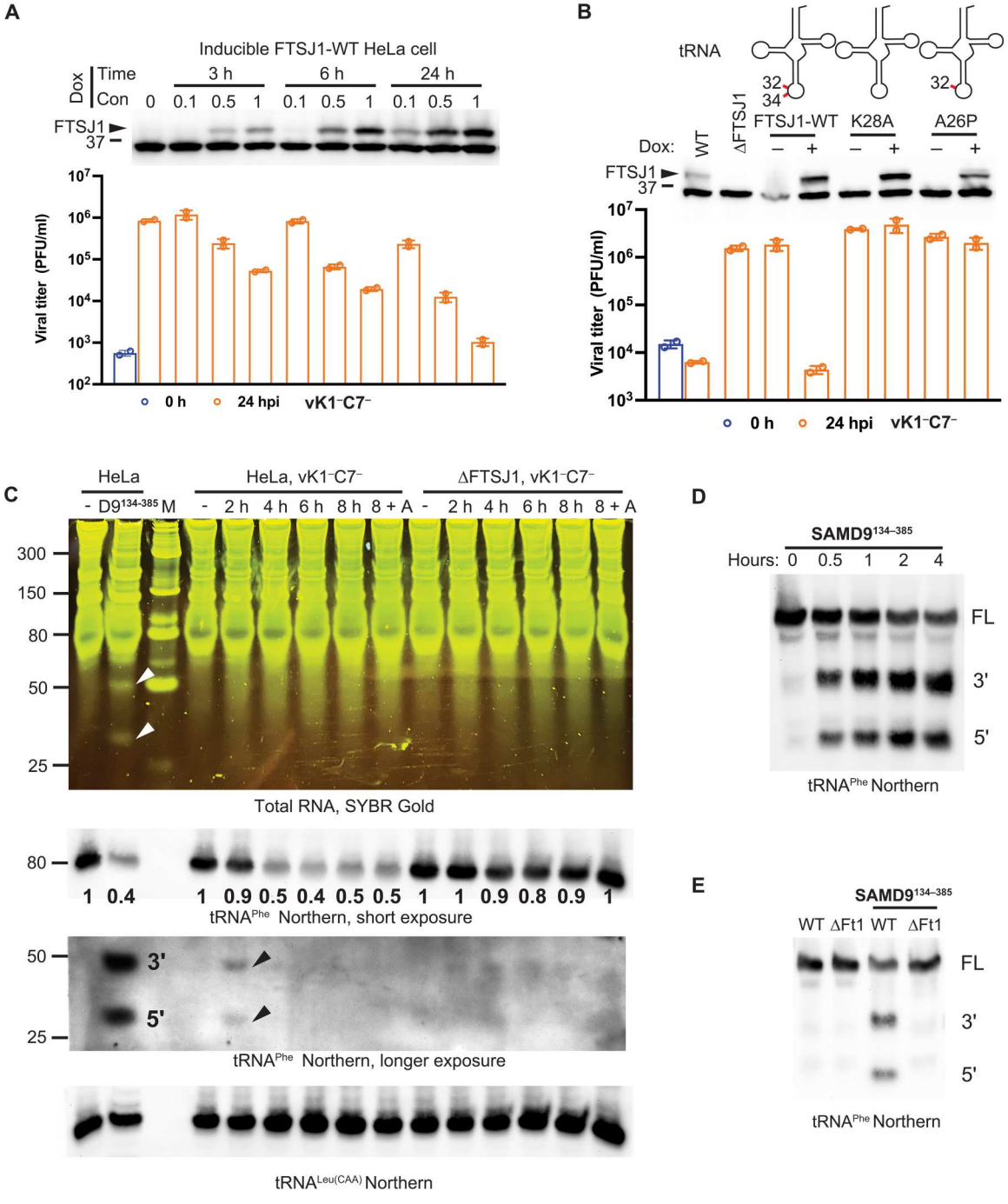

Fig. 1. SAMD9 is a VACV-activatable endoribonuclease specifically targeting tRNA^{Phe}. (**A**) HeLa cells with a Dox-inducible *FTSJ1*–wild type (WT) allele were induced to express different amount of FTSJ1 with varied Dox concentrations (0.1 to 1 μg/ml) for various time (3 to 24 hours). The FTSJ1 protein (arrowhead) and a nonspecific protein were detected by the anti-FTSJ1 antibody. The position of the 37-kDa molecular weight (MW) marker is shown. The abilities of the cells to restrict a SAMD9-sensitive mutant VACV (vK1^{-}C7^{-}) were determined by measuring the viral titers [plaque-forming units (PFU) per milliliter] at 0 and 24 hours postinfection (hpi) with plaque assays on Vero cells. (**B**) HeLa cells were engineered to express no FSTJ1 (ΔFTSJ1) or different FTSJ1 mutants under a Dox-inducible promoter. FTSJ1-K28A mutant is catalytically inactive, while FTSJ1-A26P mutant is defective of methylating at position 34 of certain tRNAs. 2′-*O*-methylations are indicated by the red lines in the tRNA schematics. (**C**) WT and ΔFTSJ1 HeLa cells were infected with vK1^{-}C7^{-} for the indicated time (2 to 8 hours). 8 + A, infection for 8 hours in the presence of cytosine arabinoside (AraC). Separately, total RNAs from uninfected HeLa cells were incubated with recombinant SAMD9$^{134–385}$ protein. RNAs resolved on a denaturing gel were stained with SYBR Gold. Lane M contains an RNA ladder, the sizes of which (in bases) are indicated on the left. Northern blots were performed with two probes complementary to 5′ or 3′ end of tRNA^{Phe} or one probe complementary to 3′ end of tRNA$^{Leu(CAA)}$. Numbers below the gel are relative band intensities with respect to that in uninfected cells. Black or white arrowheads point to the tRNA^{Phe} cleavage products. (**D**) Total RNAs from HeLa cells were incubated with SAMD9$^{134–385}$ protein for the indicated time (0.5 to 4 hours). FL, full-length tRNA. (**E**) Total RNAs from HeLa (WT) or ΔFTSJ1 (ΔFt1) cells were incubated with SAMD9$^{134–385}$ protein for 1 hour.

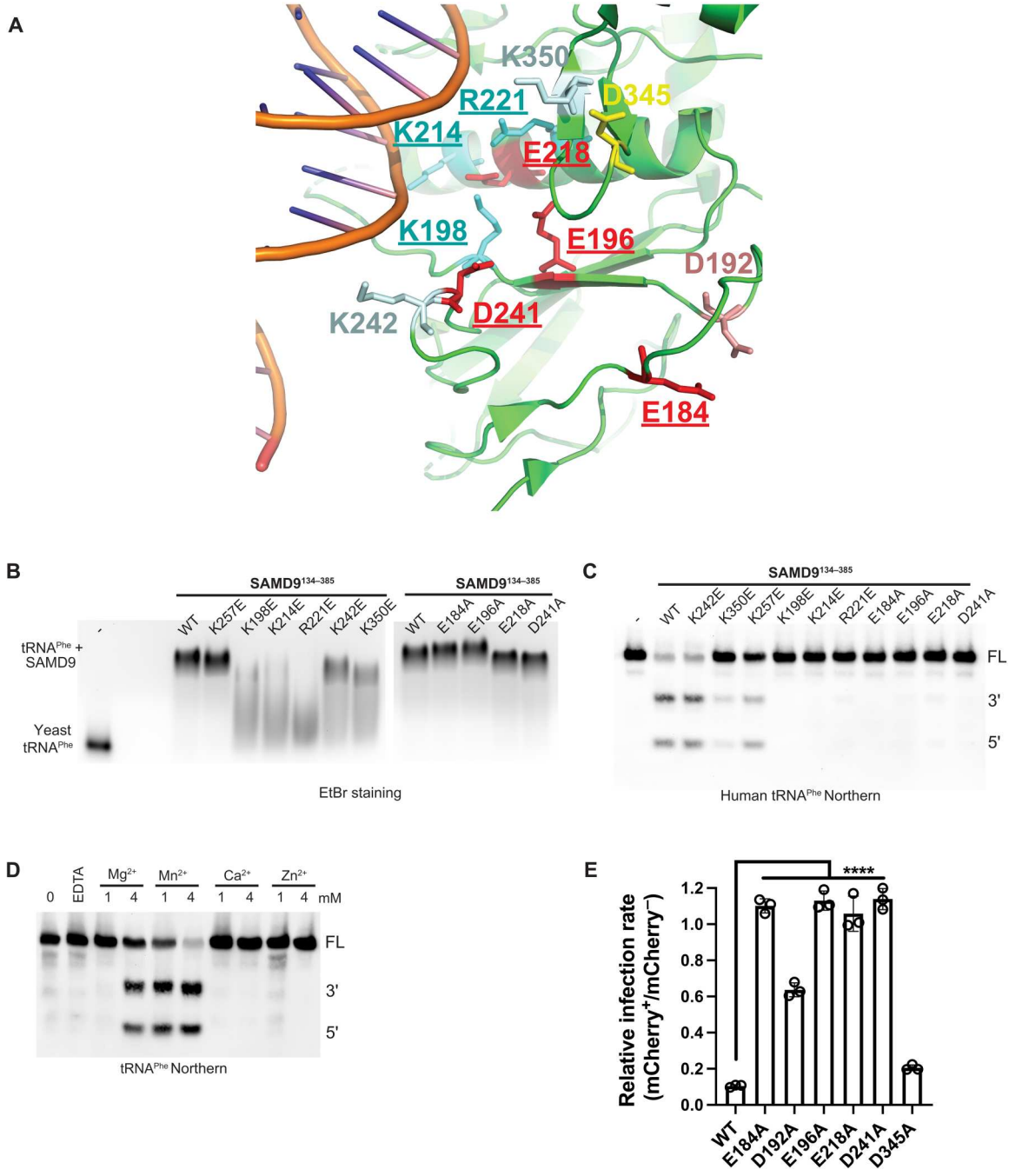

Fig. 2. tRNA binding and active site of SAMD9$^{134–385}$. (**A**) Part of the crystal structure of SAMD9$^{156–385}$/DNA complex (Protein Data Bank, 7ksp) is shown with residues that have been targeted for mutagenesis depicted. Residues that are essential for SAMD9$^{134–385}$ cleavage of tRNA^{Phe} are underlined with putative binding and active site residues colored in cyan and red, respectively. (**B**) Effects of the mutations on SAMD9$^{134–385}$ binding of yeast tRNA^{Phe} in a gel mobility shift assay. Purified SAMD9$^{134–385}$ proteins were incubated with yeast tRNA^{Phe} at 2:1 molar ratio and ran on an agarose gel. Ethidium bromide (EtBr)–stained gel is shown. (**C**) Effects of the mutations on SAMD9$^{134–385}$ cleavage of human tRNA^{Phe}. Total RNAs from HeLa cells were incubated with SAMD9$^{134–385}$ protein for 1 hour. tRNA^{Phe} fragments were detected by Northern blot. (**D**) Divalent cation requirements for SAMD9$^{134–385}$ activities. Total RNAs from HeLa cells were incubated with SAMD9$^{134–385}$ in the presence of the indicated concentrations (1 or 4 mM) of cations for 1 hour. tRNA^{Phe} fragments were detected by Northern blot. FL, full-length tRNA. (**E**) The effect of the mutations on SAMD9 antiviral activities. Human embryonic kidney (HEK) 293T cells were transfected with mCherry-SAMD9 fusions for 36 hours and infected with vK1^{-}C7^{-}/GFP^{+} for 15 hours. Infection rates (GFP^{+}%) among SAMD9-expressing and nontransfected control cells from the same culture well were simultaneously determined with flow cytometry. Relative infection rates between SAMD9-expressing and nontransfected cells are derived from the flow cytometry data shown in fig. S2B. Statistics: one-way ANOVA compared to the WT (****$P < 0.0001$).

$tRNA^{Phe}$, which is the phosphodiester 5′ to the first nucleotides of the anticodon loop.

To determine the tRNase SA substrate specificity, we focused initially on regions conserved between human and yeast $tRNA^{Phe}$, which include the D arm and most of the anticodon arm (fig. S3A). tRNase SA efficiently cleaved a 38-nt synthetic RNA, containing only the D arm, the anticodon arm, and the variable loop, at the phosphodiester 5′ to the anticodon loop (Fig. 3A). The 3′ cleavage product was readily degraded by yeast exonuclease Xrn-1 (Fig. 3B), confirming that it has the 5′ monophosphate, which is required for Xrn-1 degradation. Deletion of the variable loop or base substitutions of the anticodon stem or the last two positions of the anticodon did not affect the cleavage efficiency or the cleavage site (fig. S3B). Last, a 17-nt synthetic RNA containing only the anticodon arm was found to be efficiently cleaved at 5′ to the anticodon loop (fig. S3C). Notably, these RNAs were all synthesized with 2′-*O*-methylation at the wobble position but lack all other modifications in human $tRNA^{Phe}$ (fig. S3A).

We further assessed the substrate specificity of tRNase SA using additional synthetic variants of the 17-nt RNA. The absence of 2′-*O*-methylation at the wobble position greatly reduced cleavage, even if the position corresponding to $tRNA^{Phe}$ C32 was 2′-*O*-methylated (Fig. 3C). A 17-nt linear RNA incapable of forming a stem was not cleaved, while a 13-nt RNA forming just a stem of 3 base pairs (bp) was cleaved (Fig. 3D). Substituting the wobble base with pyrimidines greatly reduced cleavage, while substituting its adjacent position with any bases had no negative impact (Fig. 3E). Unlike metal-independent RNases (*29*), 2′-OH immediate 5′ to the scissile phosphodiester was not required for the cleavage, but substituting ribose with deoxyribose in the stem or the loop abolished the cleavage (fig. S3F). These and additional results in fig. S3 (E and F) collectively showed that tRNase SA cleaves an RNA stem loop with the feature shown in Fig. 3F: (i) a loop of 7 or 8 nt and a stem of at least 3 bp, (ii) a pyrimidine base at the first position of the loop, and (iii) a 2′-*O*-methylated purine base at the third position of the loop (corresponding to wobble position). The substrate specificity of tRNase SA therefore fully explains the exquisite specificity of SAMD9 on $tRNA^{Phe}$ and the requirement of FTSJ1 for SAMD9 activity, as $tRNA^{Phe}$ is the only tRNA that is known to have the 2′-*O*-methylated purine at position 34. Other eukaryotic tRNAs known or suspected to be methylated by FTSJ1 at position 34, including $tRNA^{Trp(CCA)}$ and $tRNA^{Leu(CAA)}$, have a pyrimidine base at the wobble position.

To further delineate the boundary of the tRNase SA domain, we tested a more compact domain of SAMD9, $SAMD9^{156–385}$, which removes 22 amino acids from the N terminus of $SAMD9^{134–385}$. In addition, to expand our study to SAMD9L, we expressed and purified the corresponding fragment of SAMD9L, $SAMD9L^{158–388}$. Both $SAMD9^{156–385}$ and $SAMD9L^{158–388}$ cleaved the natural $tRNA^{Phe}$ and the 38-nt synthetic substrate (fig. S3, G to I).

SAMD9 depletes cellular $tRNA^{Phe}$ and causes codon-specific ribosomal pausing

To comprehensively evaluate the effect of SAMD9 on intracellular tRNAs, we used a modified tRNA sequencing approach to quantify tRNA levels in cells infected with VACV. Relative to cells infected with WT VACV, $vK1^{-}C7^{-}$ infection markedly reduced the level of $tRNA^{Phe}$ by nearly 10-fold, but not other tRNAs (Fig. 4A and fig. S4A). We next conducted ribosome profiling [ribosome sequencing (Ribo-seq)] to determine the impact of $tRNA^{Phe}$ depletion on global protein synthesis. With superior 3-nt periodicity of ribosome footprints, ribosome positions can be determined with high precision as evidenced by prominent peaks at start and stop codons (fig. S4B). We calculated the A-site ribosome occupancy at individual codons by averaging the read density from the entire transcriptome. This analysis revealed a marked increase in the read density at two Phe codons UUU (~3.6-fold) and UUC (~2.6-fold) that are decoded by the single $tRNA^{Phe}$, in cells infected with $vK1^{-}C7^{-}$, relative to that in cells infected with WT VACV or uninfected cells (fig. S4D). To avoid the cascading effect of viral replication on cell physiology and to synchronize WT and $vK1^{-}C7^{-}$ VACV replication at the early stage (fig. S5B), we repeated the experiments by conducting virus infection in the presence of AraC to block viral DNA replication. Under this condition, the elevated read density at both Phe codons became more prominent in cells infected with $vK1^{-}C7^{-}$ (~5.8-fold for UUU and ~3.6-fold for UUC) (Fig. 4B).

To substantiate this finding further, we performed additional studies on BT20 cells with Dox-inducible expression of WT SAMD9 or a GoF mutant $SAMD9^{R1293W}$ that we characterized recently (*18*). Without virus infection, the expression of $SAMD9^{R1293W}$, but not WT SAMD9, decreased cellular $tRNA^{Phe}$ level by ~50% with Northern blot analysis (Fig. 4C). The level of $tRNA^{Leu(CAA)}$ remained comparable, supporting the specificity of tRNA targeting by SAMD9. Furthermore, we tested additional GoF SAMD9/9L variants in 293T cells, including R982C and E1136Q of SAMD9, as well as W1180R and F886Lfs*11 of SAMD9L, by transient transfection in 293T cells. All the GoF variants that we tested depleted $tRNA^{Phe}$ but had little effect on $tRNA^{Leu(CAA)}$ (fig. S4, E to H). A single substitution in the effector domain (R221E or R223E) that disrupted $tRNA^{Phe}$ binding in vitro also prevented the GoF variants from depleting $tRNA^{Phe}$. Mutations of other tRNA binding residues and the putative catalytic site also prevented $SAMD9^{R982C}$ from depleting $tRNA^{Phe}$ (fig. S4E).

We performed Ribo-seq analysis on BT20 cells with Dox-inducible expression of $SAMD9^{R1293W}$. The two Phe codons UUU and UUC showed a marked increase of read density at the A-site (~8.6- and 5.3-fold, respectively) upon Dox treatment (Fig. 4D). Similar to $vK1^{-}C7^{-}$ infection, the pausing at the UUU codon was greater than at the UUC codon, presumably because the relatively weaker binding affinity of the UUU codon with $tRNA^{Phe}$, due to the non–Watson-Crick U:G base pairing at the wobble position, makes it more vulnerable to $tRNA^{Phe}$ depletion.

Activated SAMD9 triggers ribotoxic stress

To find out the common signaling cascade downstream of SAMD9 activation, we performed transcriptome analysis on the infected HeLa cells and compared it to previous results from a GoF SAMD9 variant (Fig. 5A and fig. S5A). $SAMD9^{R1293W}$ was previously shown to significantly induce 41 genes that are mostly associated with proteotoxic stress response (*18*). Nine of the 41 genes were also induced by more than fourfold in response to infection by $vK1^{-}C7^{-}$ but not by WT VACV (Fig. 5A). Among the nine genes, activating transcription factor 3 (ATF3) was induced the most with an increase of >60-fold. This was validated by reverse transcription quantitative polymerase chain reaction (RT-qPCR) analysis, which additionally showed that the ATF3 induction in infected cells requires SAMD9 and partially requires FTSJ1 (Fig. 5B).

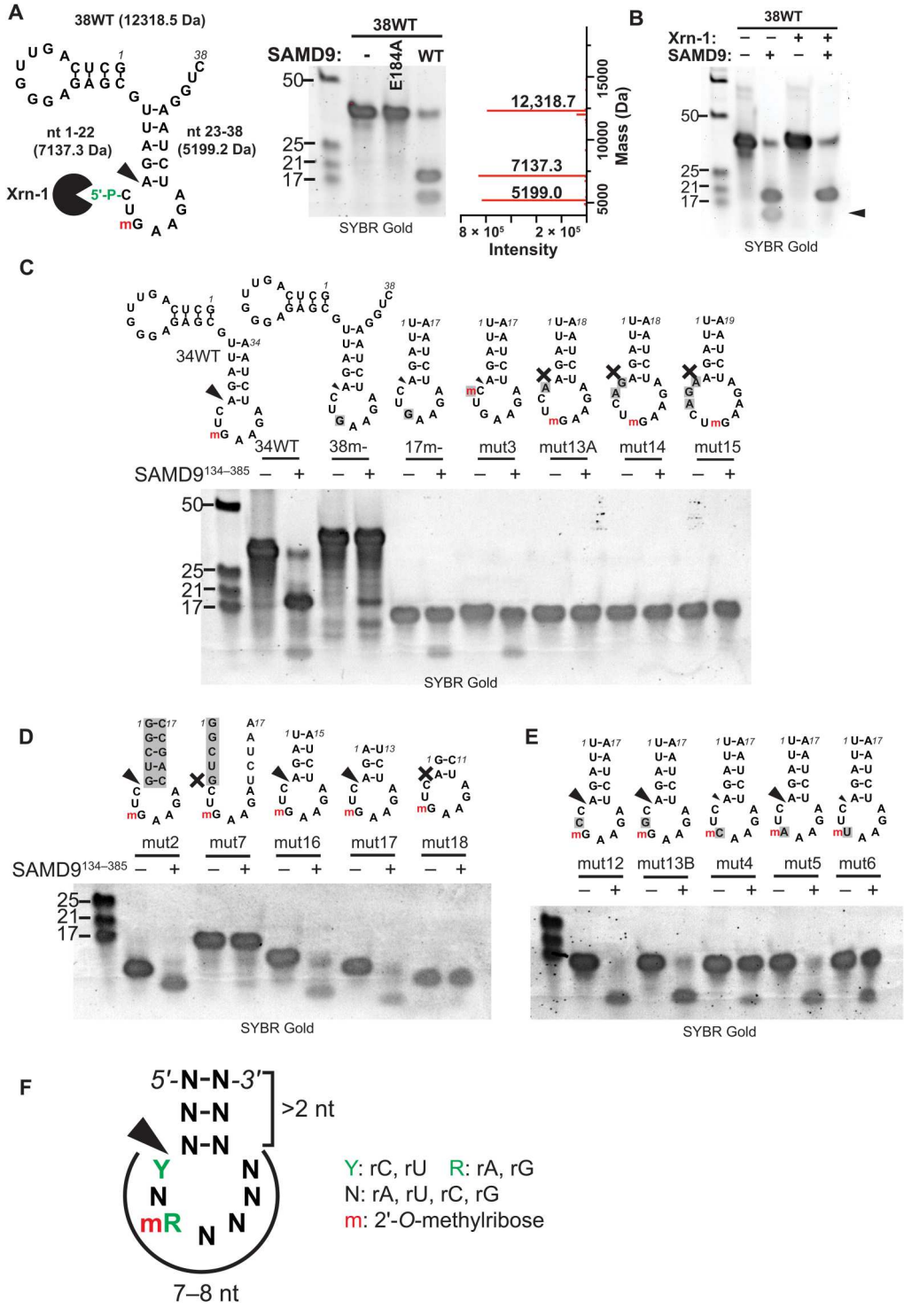

Fig. 3. SAMD9$^{134–385}$ is an ACNase with a specificity for the eukaryotic tRNA^{Phe}. (**A**) A 38-nt synthetic RNA with the depicted secondary structure was incubated with SAMD9$^{134–385}$ (WT or E184A) for 1 hour. The black arrowhead points to the cleavage site. MWs of different fragments are listed. The Xrn-1 symbol indicates that the 3′ fragment can be degraded by Xrn-1. m, 2′-*O*-methylation. The cleavage products were resolved on a denaturing gel and visualized after SYBR Gold staining. The sizes of the RNA ladder (in bases) are shown on the left of the gel. The cleavage products were analyzed with electrospray ionization liquid chromatography mass spectroscopy. The relative intensity and the MWs of the RNA species are shown. (**B**) The cleavage reaction was performed in the absence or presence of Xrn-1. The black arrowhead points to the 3′ product that disappeared in the presence of Xrn-1. Note that the RNA was synthesized with a 5′-OH group. (**C** to **E**) Synthetic RNAs with the depicted sequences were incubated with SAMD9$^{134–385}$ for 1 hour. Sequences that differ from that of tRNA^{Phe} were shown in gray background. The size of the arrows reflects the relative cleavage efficiency. "X" indicates no cleavage. (**F**) The consensus RNA structure cleaved by SAMD9$^{134–385}$.

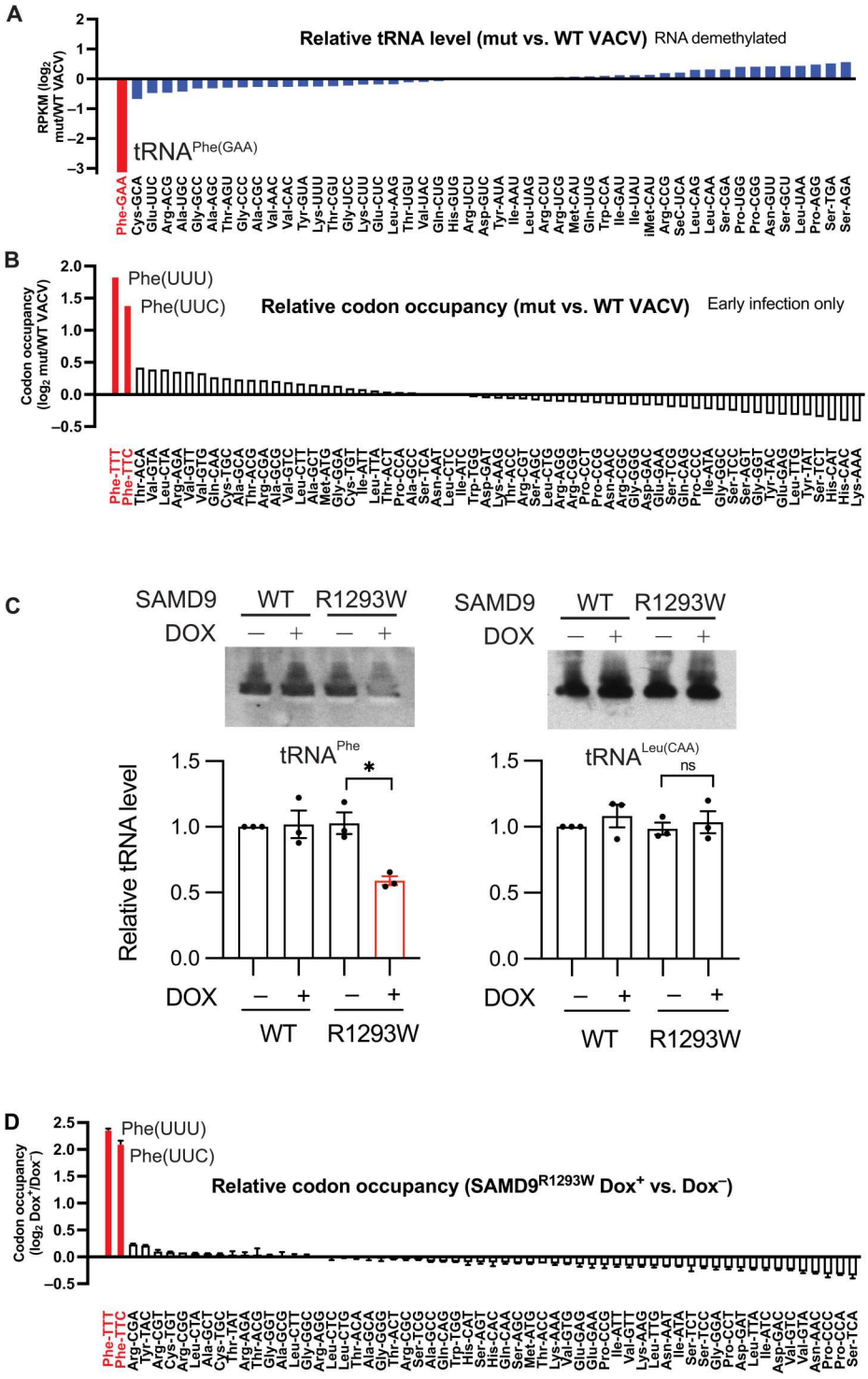

Fig. 4. SAMD9 activated by VACV or through a GoF mutation specifically depletes cellular tRNA^{Phe} and causes ribosomal pausing at Phe codons. (**A**) HeLa cells were uninfected or infected with either WT or vK1^{-}C7^{-} VACV for 8 hours. tRNAs were isolated from total RNAs resolved on a denaturing gel, treated with a tRNA demethylase and subjected to tRNA-seq. Levels of different tRNA species in vK1^{-}C7^{-}-infected cells with respect to that in WT VACV–infected cells are ranked from the lowest to the highest. tRNA^{Phe} is highlighted in red. (**B**) HeLa cells were infected as in (A) but in the presence of AraC to limit the infection to the early phase. Ribosome sequencing (Ribo-seq) was conducted, and global codon occupancy of all cellular transcripts was analyzed. Codon occupancies in vK1^{-}C7^{-}-infected cells with respect to that in WT VACV–infected cells are ranked from the highest to the lowest. Phe codons are shown in red. (**C**) BT20 cell lines with a Dox-inducible SAMD9 allele (WT or SAMD9^{R1293W}) were either uninduced or induced with Dox for 24 hours. tRNA^{Phe} and tRNA$^{Leu(CAA)}$ levels in the cells were determined by Northern blot. The graph summarizes the results from three biological replicates. ns, not significant. (**D**) BT20 cells with a Dox-inducible SAMD9^{R1293W} allele were either uninduced or induced with Dox for 24 hours. Ribo-seq was conducted, and global codon occupancy of all cellular transcripts was analyzed. Codon occupancies in Dox-induced cells with respect to that in uninduced cells are ranked from the highest to the lowest. Phe codons are shown in red.

Persistent ribosome pausing is expected to cause ribosome collision and subsequent ribotoxic stress, which is characterized by increased eukaryotic translation initiation factor 2 subunit alpha (eIF2α) phosphorylation and ATF3 induction (*30*). BT20 cells with the expression of SAMD9^{R1293W} induced ATF3 expression at mRNA and protein levels (Fig. 5C and fig. S5C). Intriguingly, knocking down tRNA^{Phe} was sufficient to induce ribotoxic stress as evidenced by eIF2α phosphorylation and the up-regulated ATF3 expression (Fig. 5D). Notably, silencing tRNA^{Leu} showed minimal effects on ATF3 induction (fig. S5D), presumably due to its relative abundance.

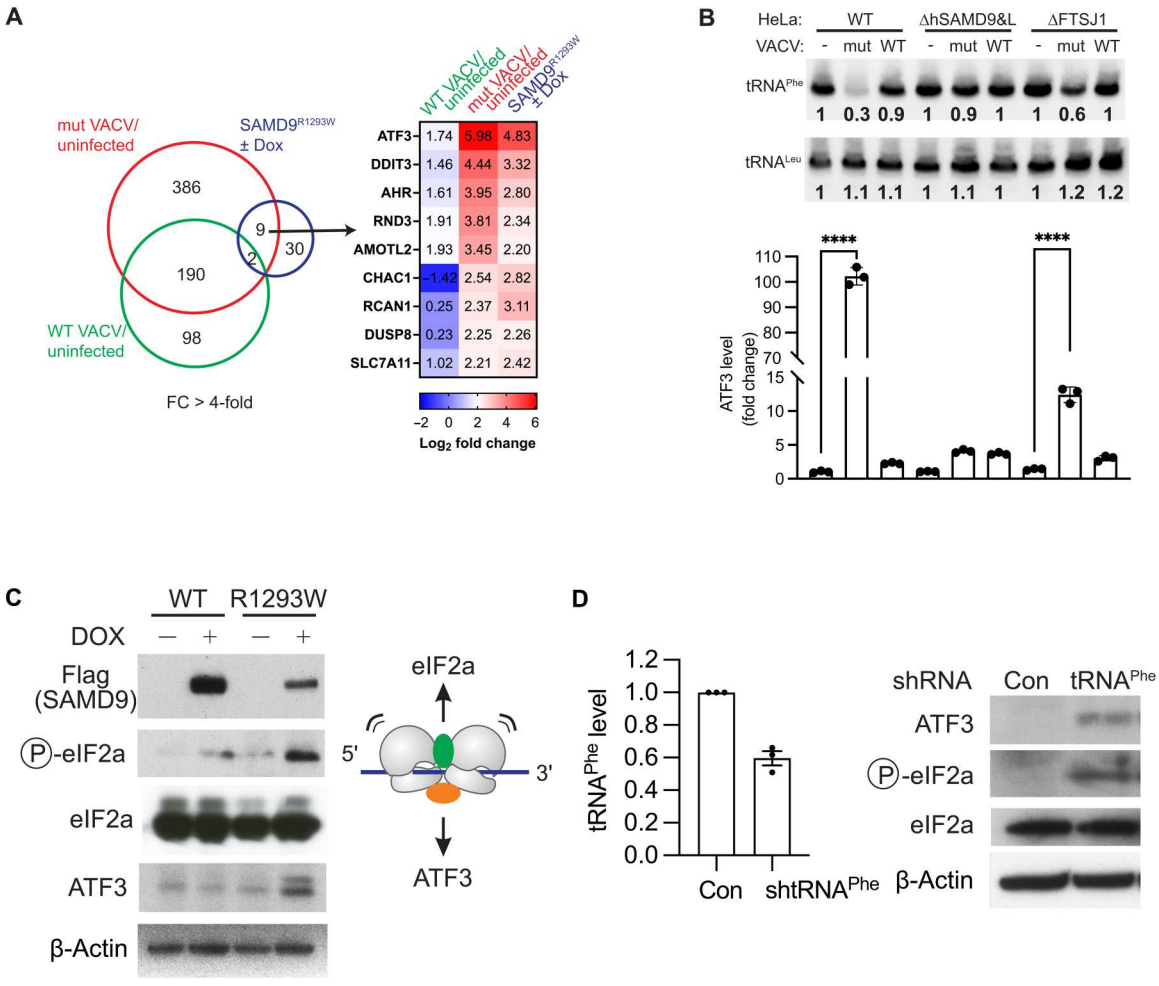

Fig. 5. Activated SAMD9 causes stress response associated with ATF3 induction. (**A**) RNA-seq was performed on HeLa cells that were uninfected or infected with either WT or vK1^{-}C7^{-} (mut) VACV for 8 hours. Numbers of genes in mut VACV and WT VACV–infected cells that showed RPKM (reads per kilobase of transcript, per million mapped reads) fold change (FC) greater than 4 with respect to uninfected cells are shown. A common set of nine genes were induced by SAMD9^{R1293W} in BT20 cells and by infection with the mut VACV (but not the WT VACV) in HeLa cells. The fold changes are shown in the heatmap. (**B**) Depletion of cellular tRNA^{Phe} and induction of ATF3 in VACV-infected cells in a SAMD9- and FTSJ1-dependent manner. HeLa cells with SAMD9 and SAMD9L KO (ΔhSAMD9&L) or FTSJ1 KO (ΔFTSJ1) were infected with vK1^{-}C7^{-} or WT VACV for 8 hours. tRNA^{Phe} and ATF3 levels in the cells were determined by Northern blot and reverse transcription quantitative polymerase chain reaction (RT-qPCR), respectively. ATF3 level is normalized with a mitochondrial mRNA level in the cells. (**C**) SAMD9^{R1293W} induces ATF3 expression and eIF2a phosphorylation. BT20 cell lines with a Dox-inducible SAMD9 allele (WT or SAMD9^{R1293W}) were either uninduced or induced with Dox for 24 hours. Proteins were detected with the indicated antibodies in immunoblots. (**D**) Knockdown of cellular tRNA^{Phe} induces ATF3 expression. Short hairpin RNA (shRNA) against tRNA^{Phe} was transduced into BT20 cells. tRNA^{Phe} level was determined by RT-qPCR, and ATF3 and phosphorylated eIF2a levels were determined by immunoblots.

Overexpression of tRNA^{Phe} restores protein synthesis and viral replication

We next tested whether SAMD9/9L–mediated inhibition of protein synthesis and VACV replication can be alleviated by overexpression of tRNA^{Phe}. To assess protein synthesis at single-cell level, we fluorescently labeled nascent cellular proteins with a puromycin analog and performed flow cytometry analysis. As we showed previously (*18*), transfection of mCherry-SAMD9^{R982C} fusion into 293T cells resulted in a strong inhibition of cellular protein synthesis in transfected (mCherry^{+}) cells, relative to nontransfected cells (mCherry^{-}) from the same culture well (Fig. 6A). Cotransfection of a plasmid overexpressing tRNA^{Phe} significantly increased cellular protein synthesis, including the synthesis of mCherry-SAMD9^{R982C} itself, in transfected cells (Fig. 6C). In comparison, cotransfection of a plasmid overexpressing tRNA^{Leu} had a minor effect (Fig. 6B). The effect of tRNA^{Phe} on cellular protein synthesis could also be detected from the total cell population by Western blot of puromycin-labeled proteins (fig. S6C).

To quantify the antiviral activity, 293T cells transfected with mCherry-SAMD9^{R982C} were infected with vK1^{-}C7^{-} and analyzed by flow cytometry. The antiviral activity of SAMD9^{R982C} was reflected by ~10-fold reduction in infection rate in mCherry-SAMD9^{R982C}–expressing cells relative to that in nontransfected cells from the same culture well (Fig. 6, E and N). Cotransfection of the tRNA^{Phe} plasmid increased the relative infection rate in transfected cells by ~60% (Fig. 6, G and N), although the cellular level of mCherry-SAMD9^{R982C} was more than doubled by tRNA^{Phe} overexpression (Fig. 6, G and M), indicating that the antiviral activity of

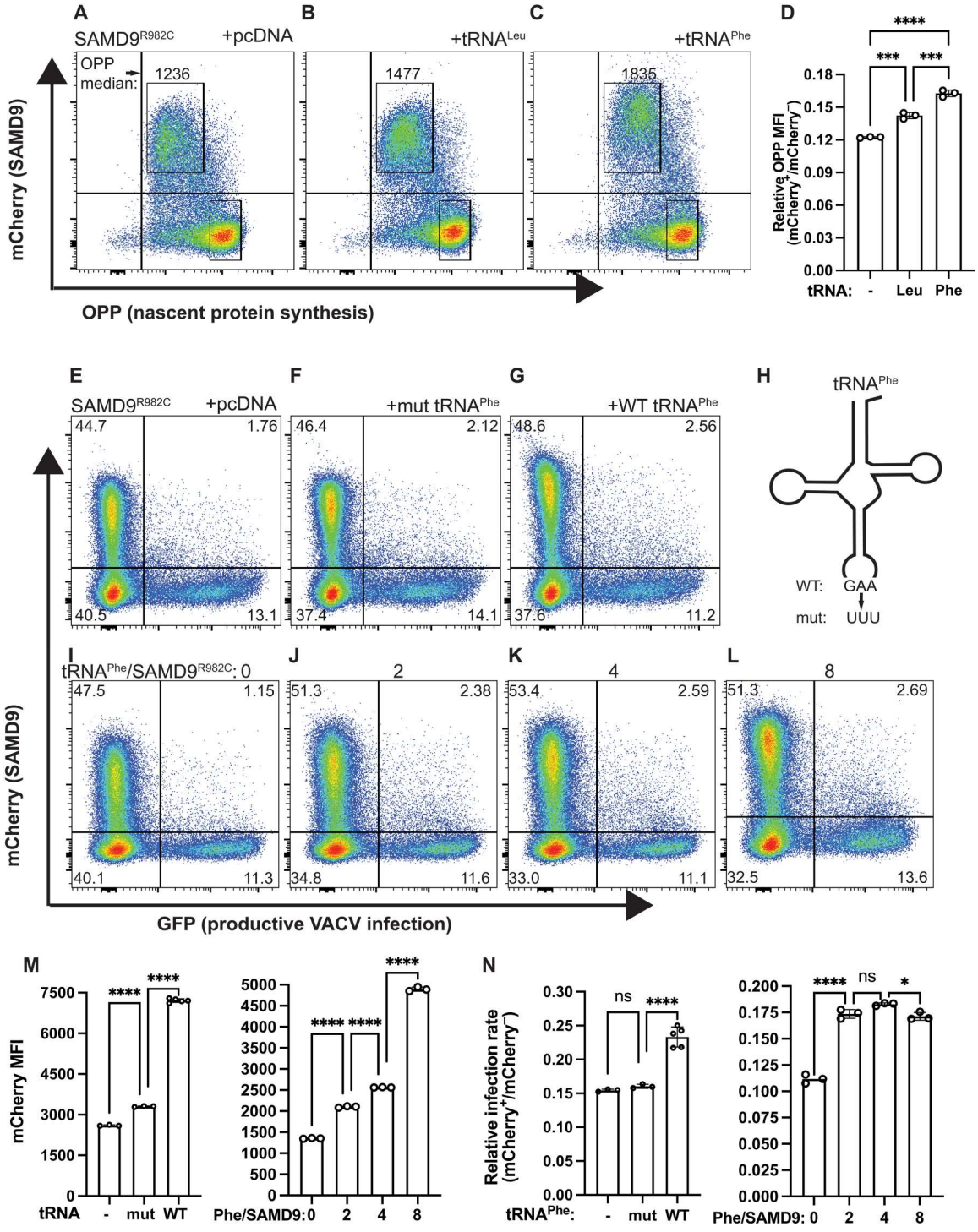

Fig. 6. Overexpression of tRNA^{Phe} reduces SAMD9 activities. (**A** to **C**) SAMD9 inhibition of global protein synthesis was reduced by tRNA^{Phe} overexpression. HEK 293T cells were transfected with mCherry-SAMD9^{R982C} and a plasmid expressing tRNA^{Phe} or tRNA^{Leu} and labeled with *O*-propargyl-puromycin (OPP) for 30 min. Representative flow cytometry plots of OPP level relative to cellular mCherry level are shown. The OPP median fluorescence intensities in SAMD9-expressing cells are listed. (**D**) Nascent protein synthesis levels in SAMD9^{R982C}-expressing cells relative to nontransfected cells from the same culture wells are derived from the flow cytometry. (**E** to **L**) SAMD9 inhibitions of protein synthesis and viral replication were reduced by tRNA^{Phe} in a dose-dependent manner. HEK 293T cells were cotransfected with a plasmid expressing mCherry-SAMD9^{R982C} and a plasmid expressing tRNA^{Phe} or a mutant tRNA^{Phe} and infected with vK1^{-}C7^{-}/GFP^{+}. Infections among SAMD9-expressing and nontransfected control cells from the same culture well were simultaneously determined with flow cytometry. Representative flow cytometry plots are shown. (**M**) The mean fluorescence intensity (MFI) of mCherry-SAMD9 in transfected cells and (**N**) the relative infection rates between SAMD9-expressing and nontransfected cells are derived from the flow cytometry data. Statistics: one-way ANOVA (ns, not significant; *$P <$ 0.1; ***$P <$ 0.001; ****$P <$ 0.0001).

SAMD9^{R982C} was attenuated. A mutant tRNA^{Phe} with a 3-nt anticodon substitution had no effect on viral replication (Fig. 6, F and N). tRNA^{Phe} overexpression increased the cellular synthesis of SAMD9^{R982C} proteins in a dose-dependent manner (Fig. 6, I to M), but the increase in the relative infection rate was nearly constant (Fig. 6, I to L and N), probably because further reduction in SAMD9 antiviral activity was counterbalanced by the increased SAMD9 protein level in the same cells. Last, we obtained similar results using WT and additional GoF mutants of SAMD9/9L by showing that overexpression of tRNA^{Phe} restored protein synthesis and viral replication (fig. S6, A to C).

DISCUSSION

SAMD9/9L have recently emerged as critical antiviral factors and myeloid tumor suppressors, with studies revealing their role as host restriction factors for poxviruses (*5*–*7*) and GoF mutations in SAMD9/9L as the underlying cause for a spectrum of human diseases with myeloid involvement (*14*, *15*, *31*). SAMD9/9L are predicted to function similarly to the STAND superfamily of signaling molecules, which share a conserved tripartite domain architecture with an N-terminal effector, a central NOD, and a C-terminal sensor. Recently, we identified an N-terminal dsNA binding domain of SAMD9/9L as the effector responsible for their antiviral and antiproliferative activities (*18*). However, the precise function of this effector has remained elusive until our current study, where we found that the effector acts as an ACNase, functioning as a specific tRNA restriction enzyme that inhibits cellular protein synthesis and restricts viral replication. This discovery of an intrinsic effector function in eukaryotic STAND-like proteins is unexpected, as previously characterized eukaryotic STAND proteins all rely on adaptors to recruit additional cellular proteins to exert their effect (*23*). For instance, the prototypical STAND protein, apoptotic peptidase activating factor 1 (APAF1), a component of the apoptosome, uses a caspase activation and recruitment domain (CARD) as its effector to recruit and activate caspase 9, thereby initiating apoptosis (*32*). The reliance on an intrinsic effector may enable SAMD9/9L to mount a more rapid response to viral infections without the need for an additional signaling step. Intriguingly, recent findings have also revealed the presence of STAND proteins with intrinsic effector functions in prokaryotes (*33*). A family of bacterial STAND proteins that sense tailed phages was found to exert their antiviral functions with diverse N-terminal nucleases (*33*), making SAMD9/9L mechanistically more similar to these prokaryotic antiviral STAND proteins.

SAMD9/9L are ubiquitously expressed in various tissues (*34*), but, under normal physiological conditions in HeLa cells and presumably other cells, they do not inhibit cellular protein synthesis or degrade tRNA. Previous studies by us and others have demonstrated that frameshift mutations truncating nearly the C-terminal half of SAMD9L lead to a GoF phenotype, rendering SAMD9L constitutively active in suppressing protein synthesis (*18*–*20*). This suggests that SAMD9/9L are typically maintained in an inactive state through autoinhibition by the C-terminal half, similar to other STAND proteins involved in innate immunity. These STAND proteins are allosterically activated once their C-terminal sensors bind to specific PAMPs. Supporting this activation model, we found that SAMD9 ACNase activity is activated upon VACV infection in HeLa cells, resulting in cleavage of tRNA^{Phe} and ribosomal pausing (Figs. 1C and 4B). Although the molecular patterns that activate SAMD9 have not yet been uncovered, it is evident that they are already present during the early stage of VACV infection, even when viral genome replication is blocked, as shown by the tRNA^{Phe} degradation and ribosomal pausing under this condition (Figs. 1C and 4B). Furthermore, the aforementioned SAMD9/9L activation model is supported by the phenotypes of various GoF mutations. The mechanisms by which GoF mutations render SAMD9/9L constitutively active in inhibiting cell proliferation are not fully understood, but it is believed that these mutations eliminate self-inhibition mediated by the C-terminal half, where nearly all GoF mutations occur. All the GoF SAMD9/9L mutations that we analyzed, including frameshift and missense mutations, result in constitutive ACNase activity (fig. S4, E to H).

The utilization of ACNases to deplete essential tRNAs and thereby halt global protein synthesis represents a previously unknown antiviral and antiproliferative mechanism in multicellular eukaryotes. Recent studies have identified members of the mammalian Schlafen protein family, which include several viral restriction factors, as having an endoribonuclease domain that targets ribosomal RNA (rRNA) and/or tRNAs (*35*, *36*). Among these, human schlafen11 solely targets tRNAs, and it cleaves type II tRNAs (tRNA^{Ser} and tRNA^{Leu}) at the acceptor stem (*37*), inhibiting the synthesis of a subset of proteins with atypical codon usage, including HIV-1 proteins (*38*). In contrast, SAMD9 cleaves the essential tRNA^{Phe} at the anticodon loop, leading to the depletion of tRNA^{Phe} and inhibition of global protein synthesis. Similar mechanisms involving ACNase depletion of essential tRNAs are found in the microbial world, although the microbial ACNases differ from tRNase SA in terms of structure and substrate specificity. For example, *E. coli* PrrC contains a higher eukaryotes and prokaryotes nucleotide-binding (HEPN) domain (*39*) and cleaves tRNA$^{lys(UUU)}$ 5′ to the wobble position (*2*), *E. coli* Colicin E5 contains a barnase, EndoU, colicinD, RelE (BECR) domain and cleaves four different tRNA species 3′ to the wobble position (*40*), and enteric bacterial toxin VapC contains a PilT N-terminus (PIN) domain and cleaves tRNA^{fMET} at 3′ end of the anticodon loop (*41*). Most of these microbial ACNases produce termini with a 2′-3′-cyclic phosphate and a 5′-OH group. In contrast, tRNase SA adopts a fold that has no close match to others in the Protein Data Bank (*18*) and cleaves tRNA^{Phe} at the 5′ end of the anticodon loop, yielding termini with a 3′-OH and 5′-phosphate group. Despite these differences, SAMD9 and the microbial ACNases have the similar effects of depleting essential tRNAs and inhibiting global protein synthesis, highlighting the importance of tRNAs as regulators of protein synthesis and innate immunity in all domains of life.

Mature tRNAs are the most extensively modified RNA species in cells (*42*), although the physiological roles of the modifications are often not fully understood. The activities of SAMD9 and some microbial ACNases are influenced by different tRNA modifications at the ASLs. For instance, PrrC activity is enhanced by the presence of the 6-threonylcarbamoyl adenosine modification at position 37 (*43*), while γ-toxin activity requires the 5-methoxycarbonylmethyl-2-thiouridine modification at the wobble position (*3*). tRNase SA specificity is primarily determined by the presence of a 2′-*O*-methylated purine base at the wobble position, which is unique to eukaryotic tRNA^{Phe} and not present in other tRNAs or most of the prokaryotic tRNA^{Phe} (fig. S7). Notably, the 2′-*O*-methylation in tRNA^{Phe} is important for organismal health, as its absence leads

to slow growth in diverse yeast species (*28*) and intellectual disability in humans (*25*, *26*). Hypomodification of $tRNA^{Phe}$ in FTSJ1 KO mice selectively reduced the steady-state level of $tRNA^{Phe}$ in the brain, resulting in decreased translation of genes that are important for brain functions (*26*). Intriguingly, GoF SAMD9L mutations are associated with ataxia-pancytopenia syndrome characterized by cerebellar ataxia, raising the possibility that $tRNA^{Phe}$ deficiency could underlie the neurological manifestation of the disease. We showed that overexpression of $tRNA^{Phe}$ could restore protein synthesis and virus replication caused by GoF SAMD9/9L (Fig. 6), suggesting that restoring $tRNA^{Phe}$ levels by overexpressing $tRNA^{Phe}$ or inhibiting SAMD9/9L ACNase activity could be a potential therapeutic strategy for diseases associated with GoF SAMD9/9L mutations.

MATERIALS AND METHODS

Reagents

The following antibodies were used in the immunoblotting: anti-FTSJ1 (Santa Cruz Biotechnology, SC-390355), anti-Flag (Sigma-Aldrich, F1804), anti-ATF3 (Cell Signaling Technology, 18665S), anti–β-actin (Sigma-Aldrich, A5441), anti-phosphorylated eIF2α (Cell Signaling Technology, 3398P), anti-eIF2α (Cell Signaling Technology, 5324), and anti-puromycin antibody (Developmental Studies Hybridoma Bank, PMY-2A4). Yeast Xrn-1 [New England Biolabs (NEB), M0338], yeast tRNA (Sigma-Aldrich, R4018), the microRNA marker (NEB, N2102S), and the Low Range ssRNA Ladder (NEB, N0364S) were acquired commercially.

Viruses

WT VACV Western Reserve (WR) strain and the K1L and C7L deletion mutant ($vK1^{-}C7^{-}$) were previously described (*10*, *44*, *45*). They were propagated and titrated on Vero cells.

Cells

Vero (ATCC CCL-81) and HeLa 229 (ATCC CCL-2.1) cells were from American Type Culture Collection (ATCC). Human embryonic kidney (HEK) 293FT cells were from Thermo Fisher Scientific (catalog no. R70007). HeLa cells with SAMD9 and SAMD9L KO (ΔSAMD9&L) (*7*) and BT cells (*18*) with Dox-inducible expression of SAMD9-WT or $SAMD9^{R1293W}$ were described before.

Plasmids construction

To overexpress $tRNA^{Leu}$(CAA) in vivo, the sequence including promoter region, tRNA sequence and terminator region was amplified by PCR using genomic DNA extracted from BT20 cells as the template and cloned into EcoR I and Pst I sites of pcDNA3.1. To overexpress $tRNA^{Phe}$ in vivo, the Q5 Site-Directed Mutagenesis Kit (NEB) was used to replace the $tRNA^{Leu}$ sequence with $tRNA^{Phe}$.

To knock out FTSJ1 gene, a pair of complementary oligonucleotides (table S1) that contain the guide sequence for FTJS1 (5′-ATCTGTACCACACCTGGTAG-3′) was cloned into lenti-CRISPRv2 (Addgene, plasmid no. 52961) that had been digested with Esp3 I, essentially as described (*46*).

Lentiviral plasmids for expressing FTSJ1 were constructed by PCR amplification of a FTSJ1 complementary DNA (cDNA) clone (Transomic Technologies) and subcloning the PCR fragment into Nhe I and BamH I sites of pCW57.1 (Addgene, no. 41393), a doxycycline-inducible lentiviral vector with rtTA-VP16-2A-puro. To decrease FTSJ1 basal expression level, the minimal CMV promoter upstream of the FTSJ1 gene was modified to match that in pTRE3G-IRES vector (Takara Bio) by using a synthetic DNA fragment (Eurofins). FTSJ1 K28A and A26P mutations were introduced into the plasmid through PCR with primers containing the desired mutations (table S1) and subcloning the PCR fragments between Nhe I and EcoR I sites of the vector.

Plasmids for expressing mCherry-SAMD9/9L fusion (pcDNA6.2/mCherry-SAMD9/9L) were described previously (*18*). Specific mutations of SAMD9/9L were introduced into the plasmids through recombinant PCR-based site-directed mutagenesis as described previously (*44*).

Generation of HeLa cell lines that express FTSJ1 allele under the Dox-inducible promoter

A FTSJ1 KO HeLa cell line was first generated by transient transfection of the plasmid containing the guide sequence for FTSJ1 to HeLa cells, followed by selection with puromycin (3 μg/ml) for 2 days. Cells that survived the selection were cultured in the absence of puromycin, and multiple cell clones were isolated and tested for FTSJ1 expression by Western blotting. Cell clones that showed no FTSJ1 expression by Western blot were also tested for the FTSJ1 genotype by Sanger sequencing as described previously (*7*). The FTSJ1 KO cells were transduced with lentivirus encoding FTSJ1 WT or mutant alleles, similar as described previously (*9*). Transduced cells were selected with puromycin at 3 μg/ml.

Viral growth analysis

Cells in 12-well plates were incubated with 1 plaque-forming unit per cell of the VACV for 2 hours at room temperature. Following adsorption, the cells were washed twice with phosphate-buffered saline. One set of the cells was harvested immediately as the 0 hpi sample, while the other set was moved to 37°C incubator to initiate viral entry and harvested at 24 hpi. The viral titers in the cell lysates were determined by plaque assays on Vero cells.

Protein purification

Recombinant $SAMD9^{134–385}$, $SAMD9^{156–385}$, and $SAMD9L^{158–388}$ proteins were expressed in *E. coli* as a small ubiquitin-like modifier (SUMO) fusion with a 6xHis-tag and purified as previously described (*18*).

Assay of SAMD9/9L activities in HEK 293T cells

HEK 293T cells in 24-well plates were transfected with pcDNA6.2/mCherry-SAMD9/9L plasmids before they were subjected to the following assays. For assessing antiviral activities, cells that had been transfected for 36 hours were infected with $vK1^{-}C7^{-}/GFP^{+}$ at a multiplicity of infection of 1 for 15 hours. For assessing protein synthesis level, cells that had been transfected for 24 hours were treated with 10 μM of *O*-propargyl-puromycin (OPP) for 30 min before they were processed with the Click-iT Plus OPP Alexa Fluor 488 Protein Synthesis Assay Kit according to the manufacturer's instruction (Thermo Fisher Scientific). The cells were harvested using trypsin-EDTA solution, fixed with 4% paraformaldehyde for 20 min, washed twice with Hanks' balanced salt solution (HBSS) (Sigma Life Science) supplemented with 1% bovine serum albumin, resuspended in 400 μl of HBSS, filtered with 40-μm mesh, and analyzed with an LSR II cell analyzer (BD Biosciences). Flow data were analyzed using FlowJo software (TreeStar). Protein

synthesis rates in total transfected cells were also assessed by labeling the cells with puromycin (10 μg/ml; InvivoGen) for 10 min followed by Western blot with an anti-puromycin antibody (PMY-2A4, Developmental Studies Hybridoma Bank).

Electrophoretic mobility shift assay

The binding of the purified SAMD9 proteins with yeast tRNA was studied by electrophoretic mobility shift assay on a 0.8% native agarose gel as previously described (*18*).

In vitro cleavage assay

Total RNA (10 μg) extracted from HeLa cells or 20 pmol of synthetic RNAs (table S1) was incubated with 0.8 to 14 μg of recombinant SAMD9$^{134–385}$ protein in the cleavage buffer at 37°C for 60 min. The cleavage buffer was made of 40 mM tris-HCl (pH 8.0), 20 mM KCl, 4 mM $MgCl_2$ (or $MnCl_2$), and 2 mM dithiothreitol (DTT). The cleavage products were mixed with gel loading dye (Invitrogen, 8546G) and resolved on 8% or 15% denaturing polyacrylamide gel containing 8 M urea. The gels were stained with SYBR Gold (Invitrogen, S11494) or subjected to Northern blot analysis.

Northern blot analysis

Northern blots were performed as described (*47*). Briefly, RNAs resolved on denaturing urea-polyacrylamide gel were transferred onto a positive charged nylon membrane. RNAs on the membrane were visualized and photographed after ethidium bromide staining. The staining was washed away, and the RNAs on the membrane were cross-linked with short-wave ultraviolet light. The membrane was probed with digoxigenin (DIG)–labeled DNA oligonucleotides against specific tRNAs. The labeling of oligonucleotides was performed with a DIG oligonucleotide 3′-End labeling kit (Roche). The signal is detected with chemiluminescence with CDP-Star as the substrate (Roche).

Mass spectroscopy

Oligonucleotide mass was determined with electrospray ionization liquid chromatography mass spectroscopy by Novatia, LLC (Newtown, PA).

Immunoblotting

SDS–polyacrylamide gel electrophoresis gel (12%) was used to separate proteins with different mass, and proteins were transferred to polyvinylidene difluoride or nitrocellulose membranes (Thermo Fisher Scientific). Membranes were blocked in blocking buffer containing tris-buffered saline (TBS), 5% nonfat milk, and 0.1% Tween 20 for 1 hour at room temperature with shaking. Primary antibodies were diluted in blocking buffer (1:1000) and added to membrane overnight at 4°C. After incubation with horseradish peroxidase–coupled secondary antibodies for 1 hour at room temperature, the membrane was washed three times with Tris-buffered saline with 0.1% Tween 20 detergent (TBST), and immunoblots were visualized using enhanced chemiluminescence (ECL-Plus, GE Healthcare).

Lentiviral shRNAs

Short hairpin RNA (shRNA) sequence targeting tRNA^{Phe} (GAA) is 5′-TCAGTTGGGAGAGCGTTAGAC-3′. shRNA sequence targeting tRNA^{Leu} (CAA) is 5′-TCTAAGGCGCCAGACTCAAGT-3′. All the shRNA targeting sequences were cloned into DECIPHER pRSI9-U6-(sh)-UbiC-TagRFP-2A-Puro (Cellecta). Lenti-X 293T cells (Clontech) were used to package lentiviral particles. The supernatants containing virus were collected and filtered at 48 hours after transfection. Then, the lentivirus was added to cells for 24 hours. After selection by puromycin (2 μg/μl), tRNA knockdown cells were collected and characterized.

Reverse transcription quantitative polymerase chain reaction

For detecting mRNA levels, the cDNA was obtained by reverse transcription using the High-Capacity cDNA Reverse Transcription Kit (Invitrogen) or the iScript Select cDNA Synthesis Kit (Bio-Rad). For detecting tRNA levels, the cDNA was obtained by the rtStar tRNA-optimized First-Strand cDNA Synthesis Kit (ArrayStar). Real-time PCR was performed using the Power SYBR Green PCR Master Mix (Applied Biosystems) and run on the LightCycler 480 Real-Time PCR System (Roche Applied Science) or a CFX96 Real-Time system (Bio-Rad). Relative expression was calculated using the $2^{-\Delta\Delta Ct}$ method.

tRNA sequencing

Total RNA was deacylated in 50 mM tris-HCl (pH 9.0) at 37°C for 45 min and then resolved by 10% polyacrylamide tris-borate EDTA (TBE)–urea gel (Invitrogen). tRNA (60 to 100 nt) were collected by gel excision and resolved in RNA elution buffer [300 mM NaOAc (pH 5.2), 1 mM EDTA, SUPERase In (0.1 U/μl)] overnight. After ethanol precipitation, tRNA was treated with demethylase (rtStar tRNA-optimized First-Strand cDNA Synthesis Kit, ArrayStar) and cleaned up. tRNA (1 μg) was used for library construction. Briefly, tRNA was dephosphorylation in the 15-μl mixture containing 1 × T4 polynucleotide kinase buffer, SUPERase In (1 U/μl), and T4 polynucleotide kinase (1 U/μl) at 37°C for 30 min and followed by 65°C for 20 min. After ethanol precipitation, RNA was pelleted by centrifugation for 15 min at 20,000*g* at 4°C and dissolved in nuclease-free H_2O. Poly(A) tailing and 5′ adenylation reaction was carried in the mixture containing 1× poly(A) tailing reaction buffer, 1 mM adenosine 5′-triphosphate, SUPERase In (1 U/μl), poly(A) polymerase (1 U/μl), and Ezra (1 U/μl) (*48*) at 37°C for 30 min and followed by 65°C for 20 min. RNA sample was then mixed with 1 μl of 1 μM ligation adaptor (5′-AATGATACGGCGACCACCGAGATCTACACTCTTTCCCTACACGACGCTCTTCCGATCT rGrGrG-3′) and heated at 65°C for 2 min and then immediately put on ice for 1 min. Ligation was performed in a 5-μl mixture containing 1× T4 RNL2 reaction buffer, SUPERase In (1 U/μl), 15% PEG8000, and T4 RNA ligase 2 (20 U/μl) truncated at 22°C for 1.5 hours. For reverse transcription reaction, 1 μl of 1 μM RT primer (5′-GCATCTCGGTGGTCCAATCTGAACTCCAGTCGTGTGACTGGAGTTCAGACGTGTGCTCTTCCGATCTTTTTTTTTTTTVN-3′) was added to the ligation products and denatured at 65°C for 2 min and cooled down on ice for 1 min. The linker-ligated RNA was then mixed with 1× first strand buffer, 0.5 mM deoxynucleotide triphosphate (dNTP), 5 mM DTT, RNaseOUT (2 U/μl), and SuperScript IV (200 U/μl) at 50°C for 1 hour, followed by 80°C for 10 min. PCR was performed in a 20-μl mixture containing 1× Phusion HF buffer (NEB), 0.2 mM dNTP, 0.5 μM forward PCR primer (5′-AATGATACGGCGACCACCGAGATCTACACTCTTTCCCTACACGACGCTCT-3′), 0.5 μM reverse PCR primer with barcode (see below), and 0.5 U of Phusion polymerase. The PCR was initiated at 98°C for 30 s, then 98°C for 5 s, 68°C for 20 s, and 72°C for 15 s for 12 cycles. PCR

products were separated on a nondenaturing 8% polyacrylamide TBE gel. Expected DNA at 200 to 240 bp was excised and soaked by 400 μl of DNA elution buffer (300 mM NaCl and 1 mM EDTA) overnight. After removal of gel debris using Spin-X column, samples were ethanol precipitated and dissolved in 15 μl of nuclease-free H_2O. Last, samples were sequenced (Illumina HiSeq) by using sequencing primers: library-PCR-R-13: 5′-CAAGCAGAAGACGGCATACGAGATTGTTGACTGTGACTGGAGTTCAGACGTGTGCTCT-3′; library-PCR-R-14: 5′-CAAGCAGAAGACGGCATACGAGATACGGAACTGTGACTGGAGTTCAGACGTGTGCTCT-3′; library-PCR-R-15: 5′-CAAGCAGAAGACGGCATACGAGATTCTGACATGTGACTGGAGTTCAGACGTGTGCTCT-3′; library-PCR-R-16: 5′-CAAGCAGAAGACGGCATACGAGATCGGGACGGGTGACTGGAGTTCAGACGTGTGCTCT-3′; library-PCR-R-18: 5′-CAAGCAGAAGACGGCATACGAGATGTGCGGACGTGACTGGAGTTCAGACGTGTGCTCT-3′; library-PCR-R-19: 5′-CAAGCAGAAGACGGCATACGAGATCGTTTCACGTGACTGGAGTTCAGACGTGTGCTCT-3′; library-PCR-R-20: 5′-CAAGCAGAAGACGGCATACGAGATAAGGCCACGTGACTGGAGTTCAGACGTGTGCTCT-3′; library-PCR-R-21: 5′-CAAGCAGAAGACGGCATACGAGATTCCGAAACGTGACTGGAGTTCAGACGTGTGCTCT-3′.

Ribosome sequencing

Ribo-seq in BT20 cells was performed as follows. Ribosome fractions separated by sucrose gradient sedimentation were pooled and digested with *E. coli* RNase I (Ambion, 750 U per 100 A260 units) by incubation at 4°C for 1 hour. SUPERase inhibitor (50 U per 100 U of RNase I) was then added into the reaction mixture to stop the digestion. Total RNA was extracted using TRIzol reagent. RNA was separated on a 15% polyacrylamide TBE-urea gel (Invitrogen), and the ribosome-protected fractions were excised (25 to 35 nt). After gel soaking and RNA precipitation, RNA was collected for library construction as described above. Last, expected DNA at 160 to 180 bp was excised and collected for sequencing.

Ribo-seq in VACV-infected cells was performed essentially as described (*49*). The steps include RNase I treatment, ribosome recovery, footprint fragment purification, 3′ adaptor ligation, rRNA depletion, reverse transcription, circularization, and PCR amplification (*49*).

Alignment of sequencing reads

The 3′ adapter was trimmed by Cutadapt (*50*). Trimmed reads with length < 15 nt were excluded. For Ribo-seq and RNA sequencing (RNA-seq), the remaining reads were mapped to a household database including all putative human rRNAs by using Bowtie (*51*). Mismatch is not permitted. The reads that cannot be aligned to rRNAs were aligned to human transcriptome using STAR (*52*). To construct the transcriptome, the annotation file from the Ensembl database (GRCh38) was used. For each gene, the mRNA with the longest coding sequence (CDS) was selected. In the case of equal CDS length, the longest transcript was used. For read alignment, a maximum of two mismatches were permitted. To avoid ambiguity, reads that were mapped to multiple positions were excluded. For tRNA-seq, the adaptor-trimmed reads were aligned to human genome (GRCh38) using HISAT2 (*53*), and the reads that were aligned to the human tRNAs were extracted and then were aligned to a household tRNA database that contains a unique tRNA sequence for each type of tRNAs. Mismatch is not permitted. For the reads that can be aligned to multiple tRNAs, the read is counted as $1/n$ for each tRNA (n is the total number of tRNAs that can be aligned).

Aggregation plot of footprint reads near the start and stop codons

The ribosome P-site was defined as positions +12, +13, and + 14 from the 5′ end of the reads (the first position of the reads is recorded as 0). For each mRNA, the mRNA with total reads in the CDS < 32 was excluded from analysis. Ribosome densities at individual mRNA sites were counted and then normalized by the average ribosome density of the CDS. Ribosome densities with the same distance from the start or stop codon were averaged over the whole transcriptome.

Estimation of ribosome density on mRNAs and mRNA levels

For each mRNA, an RPKM (reads per kilobase of transcript, per million mapped reads) value was calculated and used to measure the relative ribosome density on individual mRNAs. For Ribo-seq, only the reads aligned to the CDS were used. For RNA-seq, the reads aligned to mRNAs were used. mRNAs with RPKM values < 1 were excluded.

Calculation of ribosome occupancy

For each mRNA, ribosome densities at individual codons of the CDS were normalized to the average density of the CDS. Then, ribosome occupancies at the same codons were averaged over the whole transcriptome.

Figure preparation

SAMD9/9L amino acid sequence alignment was performed with secondary-structure matching (SSM) server (*54*), and the alignment figure was created with ESPript (*55*). $tRNA^{Phe}$ modification status in different species was obtained from the RNA modification database (*56*).

Statistical analysis

Data were analyzed using GraphPad Prism 9 software. We obtained the P value of the difference between different groups by performing Student's t test and one-way analysis of variance (ANOVA). When $P < 0.05$, differences were considered statistically significant.

Supplementary Materials

This PDF file includes:

Figs. S1 to S7
Table S1

REFERENCES AND NOTES

1. H. Masaki, T. Ogawa, The modes of action of colicins E5 and D, and related cytotoxic tRNases. *Biochimie* **84**, 433–438 (2002).
2. G. Kaufmann, Anticodon nucleases. *Trends Biochem. Sci.* **25**, 70–74 (2000).
3. J. Lu, B. Huang, A. Esberg, M. J. O. Johansson, A. S. Bystrom, The *Kluyveromyces lactis* γ-toxin targets tRNA anticodons. *RNA* **11**, 1648–1654 (2005).
4. D. M. Thompson, R. Parker, Stressing out over tRNA cleavage. *Cell* **138**, 215–219 (2009).
5. J. Liu, S. Wennier, L. Zhang, G. McFadden, M062 is a host range factor essential for myxoma virus pathogenesis and functions as an antagonist of host SAMD9 in human cells. *J. Virol.* **85**, 3270–3282 (2011).
6. G. Sivan, P. Ormanoglu, E. C. Buehler, S. E. Martin, B. Moss, Identification of restriction factors by human genome-wide RNA interference screening of viral host range mutants

exemplified by discovery of SAMD9 and WDR6 as inhibitors of the vaccinia virus K1L-C7L-mutant. *MBio* **6**, e01122 (2015).
7. X. Meng, F. Zhang, B. Yan, C. Si, H. Honda, A. Nagamachi, L. Z. Sun, Y. Xiang, A paralogous pair of mammalian host restriction factors form a critical host barrier against poxvirus infection. *PLOS Pathog.* **14**, e1006884 (2018).
8. X. Meng, B. Krumm, Y. Li, J. Deng, Y. Xiang, Structural basis for antagonizing a host restriction factor by C7 family of poxvirus host-range proteins. *Proc. Natl. Acad. Sci. U.S.A.* **112**, 14858–14863 (2015).
9. F. Zhang, X. Meng, M. B. Townsend, P. S. Satheshkumar, Y. Xiang, Identification of CP77 as the third orthopoxvirus SAMD9 and SAMD9L inhibitor with unique specificity for a rodent SAMD9L. *J. Virol.* **93**, e00225-19 (2019).
10. X. Meng, J. Chao, Y. Xiang, Identification from diverse mammalian poxviruses of host-range regulatory genes functioning equivalently to vaccinia virus C7L. *Virology* **372**, 372–383 (2008).
11. G. Sivan, S. G. Glushakow-Smith, G. C. Katsafanas, J. L. Americo, B. Moss, Human host range restriction of the vaccinia virus C7/K1 double deletion mutant is mediated by an atypical mode of translation inhibition. *J. Virol.* **92**, e01329-18 (2018).
12. R. Drillien, D. Spehner, A. Kirn, Host range restriction of vaccinia virus in Chinese hamster ovary cells: Relationship to shutoff of protein synthesis. *J. Virol.* **28**, 843–850 (1978).
13. S. S. Sahoo, V. B. Pastor, C. Goodings, R. K. Voss, E. J. Kozyra, A. Szvetnik, P. Noellke, M. Dworzak, J. Stary, F. Locatelli, R. Masetti, M. Schmugge, B. De Moerloose, A. Catala, K. Kallay, D. Turkiewicz, H. Hasle, J. Buechner, K. Jahnukainen, M. Ussowicz, S. Polychronopoulou, O. P. Smith, O. Fabri, S. Barzilai, V. de Haas, I. Baumann, S. Schwarz-Furlan; European Working Group of MDS in Children (EWOG-MDS), M. R. Niewisch, M. G. Sauer, B. Burkhardt, P. Lang, P. Bader, R. Beier, I. Muller, M. H. Albert, R. Meisel, A. Schulz, G. Cario, P. K. Panda, J. Wehrle, S. Hirabayashi, M. Derecka, R. Durruthy-Durruthy, G. Gohring, A. Yoshimi-Noellke, M. Ku, D. Lebrecht, M. Erlacher, C. Flotho, B. Strahm, C. M. Niemeyer, M. W. Wlodarski, Clinical evolution, genetic landscape and trajectories of clonal hematopoiesis in SAMD9/SAMD9L syndromes. *Nat. Med.* **27**, 1806–1817 (2021).
14. J. R. Schwartz, J. Ma, T. Lamprecht, M. Walsh, S. Wang, V. Bryant, G. Song, G. Wu, J. Easton, C. Kesserwan, K. E. Nichols, C. G. Mullighan, R. C. Ribeiro, J. M. Klco, The genomic landscape of pediatric myelodysplastic syndromes. *Nat. Commun.* **8**, 1557 (2017).
15. S. Narumi, N. Amano, T. Ishii, N. Katsumata, K. Muroya, M. Adachi, K. Toyoshima, Y. Tanaka, R. Fukuzawa, K. Miyako, S. Kinjo, S. Ohga, K. Ihara, H. Inoue, T. Kinjo, T. Hara, M. Kohno, S. Yamada, H. Urano, Y. Kitagawa, K. Tsugawa, A. Higa, M. Miyawaki, T. Okutani, Z. Kizaki, H. Hamada, M. Kihara, K. Shiga, T. Yamaguchi, M. Kenmochi, H. Kitajima, M. Fukami, A. Shimizu, J. Kudoh, S. Shibata, H. Okano, N. Miyake, N. Matsumoto, T. Hasegawa, SAMD9 mutations cause a novel multisystem disorder, MIRAGE syndrome, and are associated with loss of chromosome 7. *Nat. Genet.* **48**, 792–797 (2016).
16. B. Tesi, J. Davidsson, M. Voss, E. Rahikkala, T. D. Holmes, S. C. C. Chiang, J. Komulainen-Ebrahim, S. Gorcenco, A. Rundberg Nilsson, T. Ripperger, H. Kokkonen, D. Bryder, T. Fioretos, J. I. Henter, M. Mottonen, R. Niinimaki, L. Nilsson, C. J. Pronk, A. Puschmann, H. Qian, J. Uusimaa, J. Moilanen, U. Tedgard, J. Cammenga, Y. T. Bryceson, Gain-of-function SAMD9L mutations cause a syndrome of cytopenia, immunodeficiency, MDS, and neurological symptoms. *Blood* **129**, 2266–2279 (2017).
17. D. H. Chen, J. E. Below, A. Shimamura, S. B. Keel, M. Matsushita, J. Wolff, Y. Sul, E. Bonkowski, M. Castella, T. Taniguchi, D. Nickerson, T. Papayannopoulou, T. D. Bird, W. H. Raskind, Ataxia-pancytopenia syndrome is caused by missense mutations in SAMD9L. *Am. J. Hum. Genet.* **98**, 1146–1158 (2016).
18. S. Peng, X. Meng, F. Zhang, P. K. Pathak, J. Chaturvedi, J. Coronado, M. Morales, Y. Mao, S. B. Qian, J. Deng, Y. Xiang, Structure and function of an effector domain in antiviral factors and tumor suppressors SAMD9 and SAMD9L. *Proc. Natl. Acad. Sci. U.S.A.* **119**, e2116550119 (2022).
19. E. J. Allenspach, F. Soveg, L. S. Finn, L. So, J. A. Gorman, A. B. I. Rosen, S. Skoda-Smith, M. M. Wheeler, K. A. Barrow, L. M. Rich, J. S. Debley, M. J. Bamshad, D. A. Nickerson, R. Savan, T. R. Torgerson, D. J. Rawlings, Germline SAMD9L truncation variants trigger global translational repression. *J. Exp. Med.* **218**, e20201195 (2021).
20. A. J. Russell, P. E. Gray, J. B. Ziegler, Y. J. Kim, S. Smith, W. A. Sewell, C. C. Goodnow, SAMD9L autoinflammatory or ataxia pancytopenia disease mutations activate cell-autonomous translational repression. *Proc. Natl. Acad. Sci. U.S.A.* **118**, e2110190118 (2021).
21. S. L. Mekhedov, K. S. Makarova, E. V. Koonin, The complex domain architecture of SAMD9 family proteins, predicted STAND-like NTPases, suggests new links to inflammation and apoptosis. *Biol. Direct* **12**, 13 (2017).
22. D. D. Leipe, E. V. Koonin, L. Aravind, STAND, a class of P-loop NTPases including animal and plant regulators of programmed cell death: Multiple, complex domain architectures, unusual phyletic patterns, and evolution by horizontal gene transfer. *J. Mol. Biol.* **343**, 1–28 (2004).
23. J. D. G. Jones, R. E. Vance, J. L. Dangl, Intracellular innate immune surveillance devices in plants and animals. *Science* **354**, aaf6395 (2016).
24. J. Li, Y.-N. Wang, B.-S. Xu, Y.-P. Liu, M. Zhou, T. Long, H. Li, H. Dong, Y. Nie, P. R. Chen, E.-D. Wang, R.-J. Liu, Intellectual disability-associated gene *ftsj1* is responsible for 2′-O-methylation of specific tRNAs. *EMBO Rep.* **21**, e50095 (2020).
25. M. P. Guy, M. Shaw, C. L. Weiner, L. Hobson, Z. Stark, K. Rose, V. M. Kalscheuer, J. Gecz, E. M. Phizicky, Defects in tRNA anticodon loop 2′-*O*-methylation are implicated in non-syndromic X-linked intellectual disability due to mutations in *FTSJ1*. *Hum. Mutat.* **36**, 1176–1187 (2015).
26. Y. Nagayoshi, T. Chujo, S. Hirata, H. Nakatsuka, C. W. Chen, M. Takakura, K. Miyauchi, Y. Ikeuchi, B. C. Carlyle, R. R. Kitchen, T. Suzuki, F. Katsuoka, M. Yamamoto, Y. Goto, M. Tanaka, K. Natsume, A. C. Nairn, T. Suzuki, K. Tomizawa, F. Y. Wei, Loss of Ftsj1 perturbs codon-specific translation efficiency in the brain and is associated with X-linked intellectual disability. *Sci. Adv.* **7**, eabf3072 (2021).
27. L. Kawarada, T. Suzuki, T. Ohira, S. Hirata, K. Miyauchi, T. Suzuki, ALKBH1 is an RNA dioxygenase responsible for cytoplasmic and mitochondrial tRNA modifications. *Nucleic Acids Res.* **45**, 7401–7415 (2017).
28. M. P. Guy, E. M. Phizicky, Conservation of an intricate circuit for crucial modifications of the tRNAPhe anticodon loop in eukaryotes. *RNA* **21**, 61–74 (2015).
29. W. Yang, Nucleases: Diversity of structure, function and mechanism. *Q. Rev. Biophys.* **44**, 1–93 (2011).
30. C. C. Wu, A. Peterson, B. Zinshteyn, S. Regot, R. Green, Ribosome collisions trigger general stress responses to regulate cell fate. *Cell* **182**, 404–416.e14 (2020).
31. O. Bluteau, M. Sebert, T. Leblanc, R. Peffault de Latour, S. Quentin, E. Lainey, L. Hernandez, J. H. Dalle, F. Sicre de Fontbrune, E. Lengline, R. Itzykson, E. Clappier, N. Boissel, N. Vasquez, M. Da Costa, J. Masliah-Planchon, W. Cuccuini, A. Raimbault, L. De Jaegere, L. Ades, P. Fenaux, S. Maury, C. Schmitt, M. Muller, C. Domenech, N. Blin, B. Bruno, I. Pellier, M. Hunault, S. Blanche, A. Petit, G. Leverger, G. Michel, Y. Bertrand, A. Baruchel, G. Socie, J. Soulier, A landscape of germ line mutations in a cohort of inherited bone marrow failure patients. *Blood* **131**, 717–732 (2018).
32. O. Danot, E. Marquenet, D. Vidal-Ingigliardi, E. Richet, Wheel of Life, wheel of death: A mechanistic insight into signaling by STAND proteins. *Structure* **17**, 172–182 (2009).
33. L. A. Gao, M. E. Wilkinson, J. Strecker, K. S. Makarova, R. K. Macrae, E. V. Koonin, F. Zhang, Prokaryotic innate immunity through pattern recognition of conserved viral proteins. *Science* **377**, eabm4096 (2022).
34. C. F. Li, J. R. MacDonald, R. Y. Wei, J. Ray, K. Lau, C. Kandel, R. Koffman, S. Bell, S. W. Scherer, B. A. Alman, Human sterile alpha motif domain 9, a novel gene identified as down-regulated in aggressive fibromatosis, is absent in the mouse. *BMC Genomics* **8**, 92 (2007).
35. J. Y. Yang, X. Y. Deng, Y. S. Li, X. C. Ma, J. X. Feng, B. Yu, Y. Chen, Y. L. Luo, X. Wang, M. L. Chen, Z. X. Fang, F. X. Zheng, Y. P. Li, Q. Zhong, T. B. Kang, L. B. Song, R. H. Xu, M. S. Zeng, W. Chen, H. Zhang, W. Xie, S. Gao, Structure of Schlafen13 reveals a new class of tRNA/rRNA- targeting RNase engaged in translational control. *Nat. Commun.* **9**, 1165 (2018).
36. M. Li, E. Kao, D. Malone, X. Gao, J. Y. J. Wang, M. David, DNA damage-induced cell death relies on SLFN11-dependent cleavage of distinct type II tRNAs. *Nat. Struct. Mol. Biol.* **25**, 1047–1058 (2018).
37. F. J. Metzner, S. J. Wenzl, M. Kugler, S. Krebs, K. P. Hopfner, K. Lammens, Mechanistic understanding of human SLFN11. *Nat. Commun.* **13**, 5464 (2022).
38. M. Li, E. Kao, X. Gao, H. Sandig, K. Limmer, M. Pavon-Eternod, T. E. Jones, S. Landry, T. Pan, M. D. Weitzman, M. David, Codon-usage-based inhibition of HIV protein synthesis by human schlafen 11. *Nature* **491**, 125–128 (2012).
39. V. Anantharaman, K. S. Makarova, A. M. Burroughs, E. V. Koonin, L. Aravind, Comprehensive analysis of the HEPN superfamily: Identification of novel roles in intra-genomic conflicts, defense, pathogenesis and RNA processing. *Biol. Direct* **8**, 15 (2013).
40. Y.-L. Lin, Y. Elias, R. H. Huang, Structural and mutational studies of the catalytic domain of colicin E5: A tRNA-specific ribonuclease. *Biochemistry* **44**, 10494–10500 (2005).
41. K. S. Winther, K. Gerdes, Enteric virulence associated protein VapC inhibits translation by cleavage of initiator tRNA. *Proc. Natl. Acad. Sci. U.S.A.* **108**, 7403–7407 (2011).
42. B. El Yacoubi, M. Bailly, V. de Crécy-Lagard, Biosynthesis and function of posttranscriptional modifications of transfer RNAs. *Annu. Rev. Genet.* **46**, 69–95 (2012).
43. Y. Jiang, S. Blanga, M. Amitsur, R. Meidler, E. Krivosheyev, M. Sundaram, A. C. Bajji, D. R. Davis, G. Kaufmann, Structural features of tRNALys favored by anticodon nuclease as inferred from reactivities of anticodon stem and loop substrate analogs. *J. Biol. Chem.* **277**, 3836–3841 (2002).
44. X. Meng, Y. Xiang, Vaccinia virus K1L protein supports viral replication in human and rabbit cells through a cell-type-specific set of its ankyrin repeat residues that are distinct from its binding site for ACAP2. *Virology* **353**, 220–233 (2006).
45. X. Meng, C. Jiang, J. Arsenio, K. Dick, J. Cao, Y. Xiang, Vaccinia virus K1L and C7L inhibit antiviral activities induced by type I interferons. *J. Virol.* **83**, 10627–10636 (2009).
46. N. E. Sanjana, O. Shalem, F. Zhang, Improved vectors and genome-wide libraries for CRISPR screening. *Nat. Methods* **11**, 783–784 (2014).

47. D. C. Rio, Northern blots for small RNAs and microRNAs. *Cold Spring Harb. Protoc.* **2014**, 793–797 (2014).
48. Y. Mao, L. Jia, L. Dong, X. E. Shu, S.-B. Qian, Start codon-associated ribosomal frameshifting mediates nutrient stress adaptation. *bioRxiv*, 2023.02.15.528768 (2023).
49. N. T. Ingolia, G. A. Brar, S. Rouskin, A. M. McGeachy, J. S. Weissman, The ribosome profiling strategy for monitoring translation in vivo by deep sequencing of ribosome-protected mRNA fragments. *Nat. Protoc.* **7**, 1534–1550 (2012).
50. M. Martin, Cutadapt removes adapter sequences from high-throughput sequencing reads. *EMBnet J* **17**, 10 (2011).
51. B. Langmead, C. Trapnell, M. Pop, S. L. Salzberg, Ultrafast and memory-efficient alignment of short DNA sequences to the human genome. *Genome Biol.* **10**, R25 (2009).
52. A. Dobin, C. A. Davis, F. Schlesinger, J. Drenkow, C. Zaleski, S. Jha, P. Batut, M. Chaisson, T. R. Gingeras, STAR: Ultrafast universal RNA-seq aligner. *Bioinformatics* **29**, 15–21 (2013).
53. D. Kim, B. Langmead, S. L. Salzberg, HISAT: A fast spliced aligner with low memory requirements. *Nat. Methods* **12**, 357–360 (2015).
54. E. Krissinel, K. Henrick, Secondary-structure matching (SSM), a new tool for fast protein structure alignment in three dimensions. *Acta Crystallogr. D Biol. Crystallogr.* **60**, 2256–2268 (2004).
55. P. Gouet, X. Rober, E. Courcelle, E. Courcelle, ESPript/ENDscript: Extracting and rendering sequence and 3D information from atomic structures of proteins. *Nucleic Acids Res.* **31**, 3320–3323 (2003).
56. P. Boccaletto, F. Stefaniak, A. Ray, A. Cappannini, S. Mukherjee, E. Purta, M. Kurkowska, N. Shirvanizadeh, E. Destefanis, P. Groza, G. Avşar, A. Romitelli, P. Pir, E. Dassi, S. G. Conticello, F. Aguilo, J. M. Bujnicki, MODOMICS: A database of RNA modification pathways. 2021 update. *Nucleic Acids Res.* **50**, D231–D235 (2022).

Acknowledgments: Flow cytometry data were generated in the UT Health San Antonio Flow Cytometry Shared Resource Facility (supported by NIH-NCI P30 CA054174 and UL1 TR002645). Sequencing data were generated in the UT Health San Antonio Genome Sequencing Facility (supported by NIH-NCI P30 CA054174 and 1S10OD021805-01). **Funding:** This work was supported by National Institutes of Health grant AI151638 (Y.X.). **Author contributions:** Conceptualization: Y.X. and S.-B.Q. Methodology: F.Z., Q.J., J.C., M.M., Y.M., X.M., and L.D. Investigation: F.Z., Q.J., J.C., M.M., Y.M., Z.M., and L.D. Visualization: F.Z., Q.J., J.C., M.M., Y.M., J.D., S.-B.Q., and Y.X. Funding acquisition: Y.X. Project administration: Y.X., S.-B.Q., and J.D. Supervision: Y.X., S.-B.Q., and J.D. Writing—original draft: Y.X. Writing—review and editing: F.Z., Q.J., Y.M., J.D., S.-B.Q., and Y.X. **Competing interests:** Y.X., S.-B.Q., J.D., and Z.F. are inventors on a patent application related to this work filed by the University of Texas Health Science Center. The other authors declare that they have no competing interests. **Data and materials availability:** All data needed to evaluate the conclusions in the paper are present in the paper and/or the Supplementary Materials. The Ribo-seq and RNA-seq data have been deposited to Gene Expression Omnibus with accession numbers GSE229979 and GSE230043. The materials used in the paper can be obtained from the corresponding authors pending scientific review and a completed material transfer agreement.

Submitted 17 March 2023
Accepted 2 May 2023
Published 7 June 2023
10.1126/sciadv.adh8502

ScienceAdvances

Human SAMD9 is a poxvirus-activatable anticodon nuclease inhibiting codon-specific protein synthesis

Fushun Zhang, Quanquan Ji, Juhi Chaturvedi, Marisol Morales, Yuanhui Mao, Xiangzhi Meng, Leiming Dong, Junpeng Deng, Shu-Bing Qian, and Yan Xiang

Sci. Adv. **9** (23), eadh8502. DOI: 10.1126/sciadv.adh8502

Science Advances (ISSN 2375-2548) is published by the American Association for the Advancement of Science. 1200 New York Avenue NW, Washington, DC 20005. The title *Science Advances* is a registered trademark of AAAS.